nanomaterials

MDPI

Article

Synthesis of Porous $CoFe_2O_4$ and Its Application as a Peroxidase Mimetic for Colorimetric Detection of H_2O_2 and Organic Pollutant Degradation

Lihong Wu [1], Gengping Wan [1], Na Hu [2], Zhengyi He [1], Shaohua Shi [1], Yourui Suo [2], Kan Wang [1], Xuefei Xu [1], Yulin Tang [1] and Guizhen Wang [1,*]

[1] Key Laboratory of Advanced Materials of Tropical Island Resources (Hainan University), Ministry of Education, Haikou 570228, China; wulihongm@163.com (L.W.); wangengping001@163.com (Ge.W.); 17889886009@163.com (Z.H.); gjrshao726@163.com (S.S.); wangkanhd@163.com (K.W.); 18895627261@163.com (X.X.); yulintang321@163.com (Y.T.)

[2] Key Laboratory of Tibetan Medicine Research, Northwest Institute of Plateau Biology, Chinese Academy of Sciences, Xining 810001, China; huna@nwipb.cas.cn (N.H.); yrsuo@nwipb.cas.cn (Y.S.)

* Correspondence: wangguizhen@hainu.edu.cn or wangguizhen0@hotmail.com; Tel.: +86-0898-66268172

Received: 10 May 2018; Accepted: 14 June 2018; Published: 21 June 2018

Abstract: Porous $CoFe_2O_4$ was prepared via a simple and controllable method to develop a low-cost, high-efficiency, and good-stability nanozyme. The morphology and microstructure of the obtained $CoFe_2O_4$ was investigated by X-ray diffraction (XRD), X-ray photoelectron spectroscopy (XPS), transmission electron microscopy (TEM), high-resolution TEM (HRTEM), specific surface area and pore analysis, and Raman spectroscopy. The results show that the annealing temperature has an important effect on the crystallinity, grain size, and specific surface area of $CoFe_2O_4$. $CoFe_2O_4$ obtained at 300 °C (CF300) exhibits the largest surface area (up to 204.1 m^2 g^{-1}) and the smallest grain size. The peroxidase-like activity of $CoFe_2O_4$ was further verified based on the oxidation of peroxidase substrate 3,3′,5,5′-tetramethylbenzidine (TMB) in the presence of H_2O_2. The best peroxidase-like activity for CF300 should be ascribed to its largest surface area and smallest grain size. On this basis, an effective method of colorimetric detection H_2O_2 was established. In addition, the porous $CoFe_2O_4$ was also used for the catalytic oxidation of methylene blue (MB), indicating potential applications in pollutant removal and water treatment.

Keywords: $CoFe_2O_4$; peroxidase-like activity; artificial enzyme mimetics; hydrogen peroxide

1. Introduction

Peroxidases are a kind of efficient redox enzymes that can catalyze the oxidation of enzyme substrate in the presence of H_2O_2. Owing to strong selectivity and high catalytic efficiency, they have been widely applied to various fields, such as biotechnology, chemical industry, biosensors, and immunoassays [1–3]. Unfortunately, there still exist some intrinsic drawbacks, such as being easy to denature in extreme environmental conditions, and the high cost of preparation and purification [4]. Therefore, the construction of novel and efficient artificial enzymes is very essential and has become an increasingly important focus. Over the past few decades, a vast variety of artificial enzymes have been explored to mimic the functions of natural enzyme, such as cyclodextrins, nanomaterials, DNA complexes, and Schiff base complex [5–8]. Among them, nanomaterials have attracted intensive attention because of their ease of preparation, low price, and good stability [9–13]. Additionally, the large specific surface and more activation centers of nanomaterials also greatly extend their application range [14].

To date, a large number of nanomaterials have been found to possess unexpected peroxidase-like activity (mimicking the functions of peroxidase), including Pt nanoclusters [15], $AgVO_3$ nanobelts [16], MnO_2 nanoparticles (NPs) [17–19], WO_x quantum dots [20], Ag NPs [21], V_2O_5 nanowires [22], and Fe_3O_4 magnetic nanoparticles (MNPs) [23–25]. Additionally, a series of hybrid complexes based on metal nanomaterials have been investigated as peroxidase mimetics, such as GQDs/Ag NPs [26], Au nanocomposites [27,28], and FeSe-Pt@SiO_2 nanospheres [29]. Furthermore, carbon-based nanomaterials, e.g., single-walled carbon nanotube [30], graphene oxide (GO) [6], C@Fe_3O_4 NPs [31], GQDs/CuO nanocomposites [32] were also explored to mimic the functions of naturally-occurring enzymes. In particular, magnetic nanomaterials have been widely applied in biology, medicine and environmental fields because of their low cost, better stability, ease of separation, and recyclability. For example, Wei and his co-workers reported that the Fe_3O_4 MNPs could be a highly-efficient peroxidase-like catalyst towards H_2O_2 reduction for biosensing applications [23]. Chen's group found that magnetic carbon nitride nanocomposites possessed the superior peroxidase-like catalytic activity toward H_2O_2 and glucose and can be used as an enzyme-free biosensor [33]. Feng et al., reported the controllable synthesis of monodisperse $CoFe_2O_4$ nanoparticles by the phase transfer method and applied them in the degradation of methylene blue (MB) with H_2O_2 [34].

As a kind of high stability ferromagnetism nanomaterials, $CoFe_2O_4$ have been widely applied in lithium batteries, immunoassays, environmental science, and food chemistry [35–37]. Owing to the magnetic property for easy recyclability and high catalytic performance, $CoFe_2O_4$ is expected to be a good candidate for mimicking peroxidase [38,39]. In this study, we established a simple method to prepare porous $CoFe_2O_4$ with the controllable size of nanoparticles and specific surface area. The porous $CoFe_2O_4$ exhibited the excellent peroxidase-like catalytic activity and could be used to detect H_2O_2 and degrade MB. Benefiting from simple operation and high efficiency, $CoFe_2O_4$ materials have great potential applications in environmental protection and biotechnology.

2. Materials and Methods

2.1. Reagents

3,3′,5,5′-Tetramethylbenzidine (TMB) was purchased from Macklin (Shanghai, China). $CoCl_2{\cdot}6H_2O$, $FeSO_4{\cdot}7H_2O$, oxalic acid, methylene blue (MB), ethanol, H_2O_2 (30 wt %), isopropanol alcohol (IPA, a scavenger of hydroxyl radicals •OH) and other chemicals were all of analytical reagent grade and were obtained from Guangzhou Chemical Reagent factory (Guangzhou, China). All aqueous solutions were prepared with Milli-Q water (18.2 MΩ cm).

2.2. Preparation of $CoFe_2O_4$

$CoFe_2O_4$ samples were synthesized via a facile method. In a typical procedure, 2.5 g of $CoCl_2{\cdot}6H_2O$ and 5.6 g of $FeSO_4{\cdot}7H_2O$ were dissolved in 80 mL of deionized water and then transferred into oil bath heating at 80 °C, under vigorous stirring for 1 h. Subsequently, 30 mL 1 M oxalic acid solution was heated to boiling with magnetic stirring, and then added into the above solution slowly under constant stirring to form a final black precipitation, and then cooled by ice-water mixture. The black precipitates were collected by centrifugation and washed several times with water and ethanol, and further dried at 60 °C under vacuum for 12 h. Then, the precipitates were transferred to a tube furnace, heated to 300 °C, and maintained for 1 h. The temperature was raised at a heating rate of 1 °C min^{-1} [40]. The final product was denoted as CF300. Similarly, other $CoFe_2O_4$ samples prepared at 400 °C, 500 °C, 600 °C, and 700 °C were denoted as CF400, CF500, CF600, and CF700, respectively.

2.3. Characterization of $CoFe_2O_4$

The X-ray diffraction (XRD) patterns were collected on a Bruker D8 Advance X-ray diffractometer (Bruker Inc., Karlsruhe, Germany) with Cu Kα radiation (λ = 0.154056 nm). Scanning electron microscopy (SEM) images were observed by used a Hitachi S-4800N microscope (Hitachi Inc.,

Tokyo, Japan). The transmission electron microscopy (TEM) and high-resolution TEM (HRTEM) images were taken on a JEOL JEM-2100 microscope instrument (JEOL Inc., Tokyo, Japan) at an acceleration voltage of 200 kV. The chemical composition and elemental maps of the as-prepared samples were analyzed by energy-dispersive X-ray (EDX) spectroscopy using an EDX attachment to the SEM instrument. The X-ray photoelectron spectroscopy (XPS) data were acquired using AXIS SUPRA (Shimadzu Inc., Kyoto, Japan). The UV-vis absorbance spectra were recorded using a Lambda 750 s UV-vis-NIR absorption spectrophotometer (PerkinElmer Inc., Waltham, MA, USA). The hysteresis loop of the samples was obtained using the vibrating sample magnetometer (VSM, Lakeshore 7400, Westerville, OH, USA). The specific surface areas of the $CoFe_2O_4$ were recorded based on Brunauer-Emmett-Teller (BET) equation by an automatic nitrogen adsorption pore size distribution and specific surface analyzer (ASAP 2460, Atlanta, GA, USA). Raman spectroscopy was performed on a Renishaw inVia Reflex Raman microscope (Renishaw Inc., Gloucestershire, UK) using 532 nm green laser excitation.

2.4. Peroxidase-Like Activity Assay

To investigate the peroxidase-like activity of the prepared $CoFe_2O_4$ materials, a typical catalytic oxidation experiment was performed at room temperature with 100 μg/mL CF400 in 3 mL of phosphate-buffered saline (PBS, 20.0 mM, pH 3.5), using 0.8 mM TMB, and 4.0 mM H_2O_2 as the substrate. All the reactions were monitored in time scan mode at 652 nm, right after all of the reagents were added and mixed. Control groups included CF400 (100 μg/mL) with TMB (0.8 mM), CF400 (100 μg/mL) with H_2O_2 (4.0 mM), and TMB (0.8 mM) with H_2O_2 (4.0 mM) in 20.0 mM PBS (pH 3.0), respectively.

2.5. Optimal Conditions for H_2O_2 Detection

The effect of substrate H_2O_2 concentration (0–0.1 M), CF300 concentration (0–200 μg/mL), temperature (20–40 °C), and pH (2–8) on the peroxidase-like activity of CF300 were also investigated to ascertain the optimal conditions.

2.6. Analysis of Active Species

The active species generated in the reaction were detected by adding scavengers (IPA) into the reaction solutions [16]. The specific procedure was the same as the CF300 peroxidase-like activity assay experiments.

2.7. Steady-State Kinetic Study

A steady-state kinetic experiment was performed in a 3.0 mL reaction solution (20.0 mM PBS, pH = 3.0, 25 °C) with 20 μg/mL CF300. TMB and H_2O_2 were involved in the reaction as substrates. The steady-state kinetic data were collected by varying the concentration of one substrate while keeping the other substrate concentration constant, and the kinetic value was measured in time course mode at 652 nm [32,41]. The Michaelis-Menten constant was calculated by using the Lineweaver-Burk double reciprocal according to the equation: $1/v = (K_m/V_{max})\,(1/[S]) + 1/V_{max}$ [42,43], where v is the initial velocity, K_m is the Michaelis constant, V_{max} is the maximal reaction velocity, and $[S]$ represents the concentration of the substrate.

2.8. Methylene Blue Degradation

The catalytic activity of $CoFe_2O_4$ samples was demonstrated by degrading MB in aqueous solution. In a typical reaction, 0.015 mg of CF300 was added to 50 mL MB aqueous solution (10 mg/L), then 10 mL of aqueous H_2O_2 (30 wt %) was added in the reaction mixture. At various time intervals, a small quantity of the mixture solution was separated quickly by centrifugation. Finally, the supernatants

were pipetted into a quartz cell and analyzed with UV-vis spectrophotometer to evaluate the catalytic degradation MB [41,44].

3. Results

3.1. Characterization of the $CoFe_2O_4$

The crystal structure and purity of the products were measured by XRD. Figure 1A displays XRD patterns of $CoFe_2O_4$ prepared at different temperatures. All characteristic peaks of samples match very well with the inverse spinel structure with the lattice parameters of a = 8.377 Å and c = 8.377 Å, which is consistent with the reported data (JCPDS file no. 03-0864). The synthesized temperature has a significant effect on the crystallinity of $CoFe_2O_4$. With the increase of the prepared temperature, the crystallization of samples increases obviously. Moreover, no other characteristic peaks of impurities are detected, indicating a pure phase of $CoFe_2O_4$ can be obtained using the present method. Figure 1B shows the Raman spectra of the as-synthesized samples. The low-frequency vibrations (below 600 cm^{-1}) are belonged to the motion of oxygen around the octahedral lattice site whereas the higher frequencies can be attributed to oxygen around tetrahedral sites [45,46]. In this work, the mode at 682 cm^{-1} is a characteristic of the tetrahedral site. The bands at 470 cm^{-1} and 300 cm^{-1} correspond to Co^{2+} at octahedral sites [47].

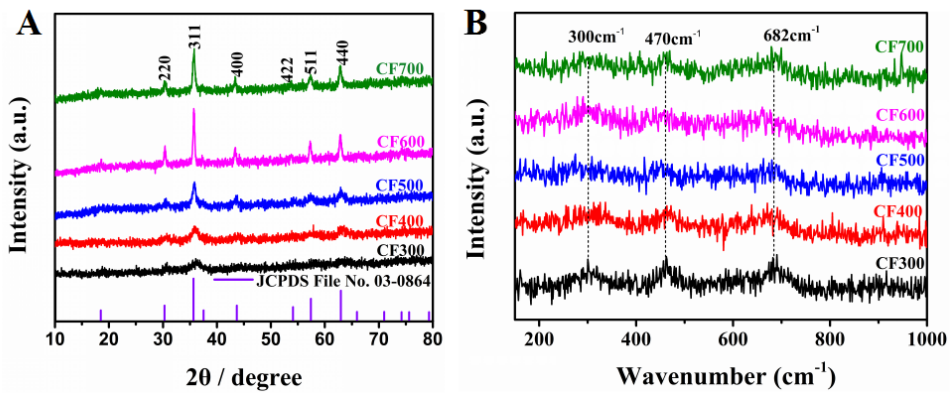

Figure 1. (**A**) XRD patterns and (**B**) Raman spectra of $CoFe_2O_4$ prepared at different temperatures.

The morphology of as-prepared $CoFe_2O_4$ is presented by SEM image. As shown in Figure 2A, CF300 show the rhombus-like polyhedron morphology with some fragments and cracks. They are several micrometers in size. Other $CoFe_2O_4$ samples obtained at different temperature also exhibit similar structure and morphology in Figure S1 (Supplementary Materials). The EDX elemental mappings (Figure 2B) and EDX spectrum (Figure S2) reveal the existence Co, O, and Fe elements. All three elements can maintain a uniform rhombus-like morphology, further demonstrating that Co, O, and Fe are homogeneously distributed in the sample.

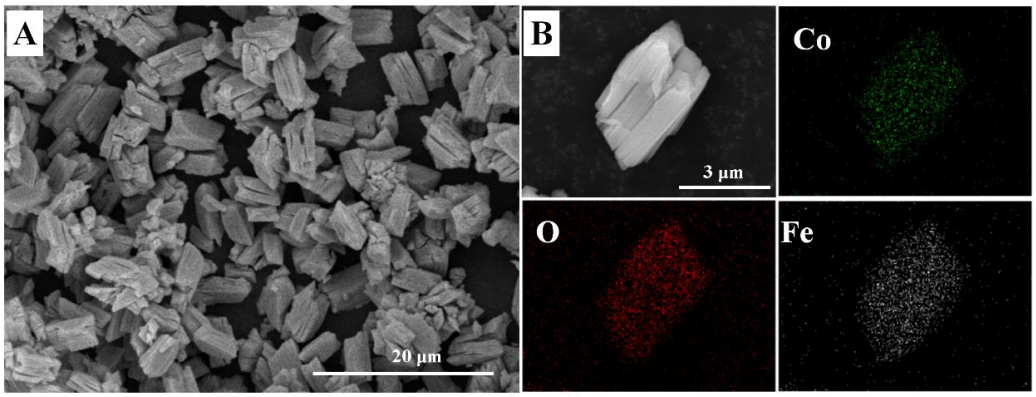

Figure 2. (**A**) SEM image of CF300 and (**B**) EDX elemental mappings.

The microstructure and morphology of the synthesized samples at different reaction temperature were further investigated by TEM. As observed from the TEM images in Figure 3A–E, all the samples exhibit a homogeneous mesoporous structure. When the synthesized temperature is increased from 300 °C to 700 °C, the pore size gradually enlarged and the pore density also decreased owing to the further crystallization and crystal growth of $CoFe_2O_4$ particles. In this work, the pores are located among the particles and mainly derived from a large amount of gases slowly release from oxalate particles during thermal decompositions [48]. Figure 3F displays the HRTEM image of CF300. The image highlights the crystalline lattice fringes with a distance of about 0.296 nm, which can be ascribed to the (220) plane of $CoFe_2O_4$. The inset in Figure 3F is the corresponding selected area electron diffraction (SAED) pattern, confirming that the sample has a monocrystalline structure. The diffraction spots can be indexed as inverse spinel-structured $CoFe_2O_4$, which is in accordance with the XRD result.

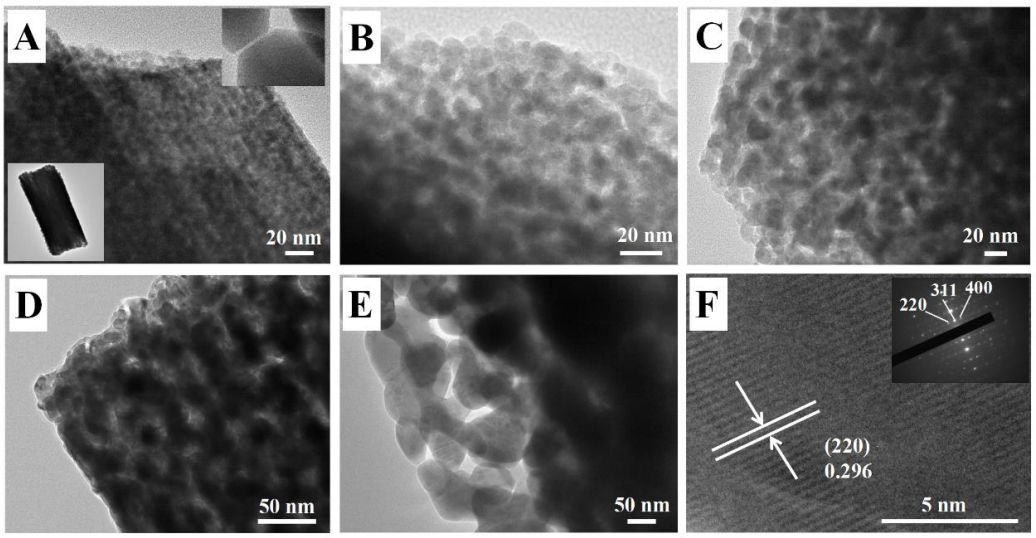

Figure 3. Typical images of (**A**) CF300; (**B**) CF400; (**C**) CF500; (**D**) CF600; and (**E**); CF700 (**F**); HRTEM image of CF300, and the inset in (**F**) is the SAED pattern.

The chemical composition and surface electronic state of the as-prepared $CoFe_2O_4$ samples were further studied by XPS. It can be seen in the XPS survey spectrum (Figure 4A) that the sample mainly contains three elements: Co, Fe, and O. The C 1s peak at around 284.8 eV could correspond to the signal from carbon contained in the instrument as calibration. In the Co 2p spectrum (Figure 4B), the peak located at about 780.58 eV corresponds to Co $2p_{3/2}$ with a satellite peak at 786.58 eV and the peak at 795.78 eV is ascribed to the Co $2p_{1/2}$. Figure 4C presents the Fe 2p orbital displaying the splitting peaks at binding energies of around 724.58 eV and 711.28 eV, which can be assigned to the

Fe $2p_{1/2}$ orbital and Fe $2p_{3/2}$ orbital, respectively. These results are well in agreement with many other reports [49,50]. Figure 4D shows the high-resolution XPS spectra of the O 1s. Based on the previous reports, the signal peak located at 530.94 eV could be assigned to typical lattice oxygen in $CoFe_2O_4$. The peak located at 531.4 eV is assigned to C–O bonds. The XPS spectrum is in good agreement with the literature [51].

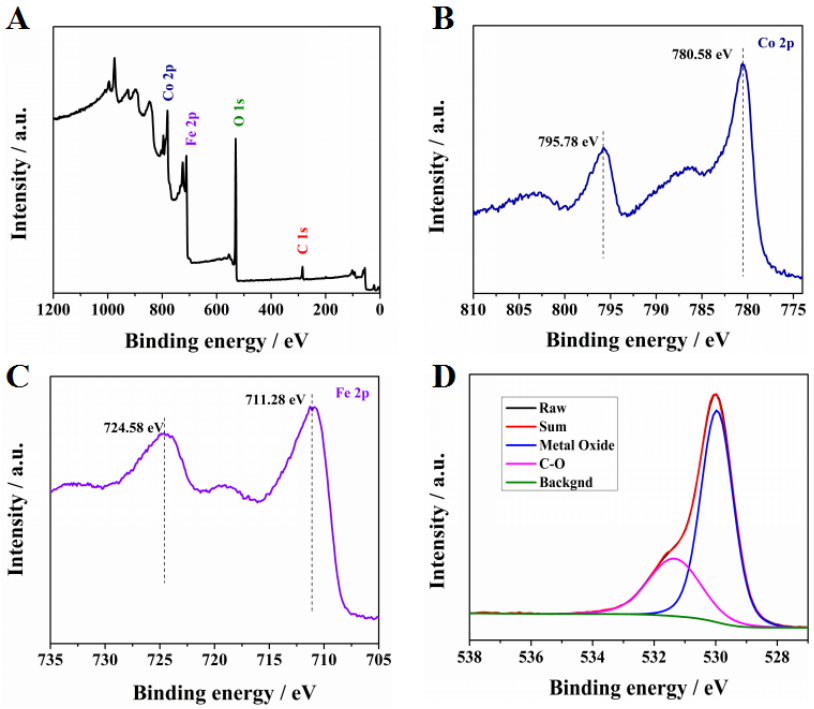

Figure 4. XPS spectra of CF300: (**A**) survey spectrum, high resolution XPS spectra of (**B**) Co 2p, (**C**) Fe 2p, and (**D**) O 1s.

N_2 adsorption/desorption isotherms of the samples are depicted in Figure 5A. Typical type IV adsorption isotherms with an H3-type hysteresis loop are observed for all samples except CF700, indicating the mesoporous feature of the $CoFe_2O_4$ nanostructures. Figure 5B shows the relevant Barrett-Joyner-Halenda (BJH) pore size distribution of the porous $CoFe_2O_4$, in which there exists a sharp maximum at 3.5–20.6 nm, further indicating the material has a mesoporous structure. The porous trait will greatly enhance the surface area and active sites, and thus improve the catalytic performance [52]. The specific surface, pore diameter, and pore volume of these samples are shown in Table 1. We can see that, as the preparing temperature increases, the obvious decrease is found for the pore volume (0.228 to 0.019 cm^3/g) and specific surface (204 to 18 m^2/g). The magnetism of CF300 sample was determined by the hysteresis loop on VSM. It can be seen in Figure S3 that CF300 displays typical ferromagnetism at room temperature. The coercivity (Hc), saturation magnetization (Ms) and residual magnetization (Mr) are about 12 Oe, 8.372 emu/g and 0.064 emu/g respectively.

Table 1. Specific surface, pore diameter, and pore volume of synthesized $CoFe_2O_4$ samples.

Sample	Specific Surface (m^2/g)	Pore Diameter (nm)	Pore Volume (cm^3/g)
CF300	204.10	4.47	0.228
CF400	112.17	8.84	0.248
CF500	58.44	14.29	0.209
CF600	21.78	5.56	0.030
CF700	18.25	4.18	0.019

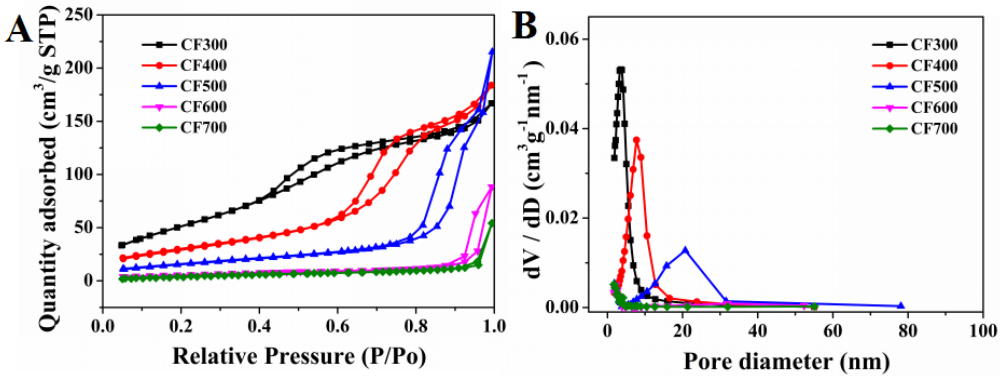

Figure 5. (**A**) N_2 adsorption/desorption isotherms and (**B**) pore size distribution of the porous $CoFe_2O_4$.

3.2. Peroxidase-Like Activity of $CoFe_2O_4$

To examine the peroxidase-like activity of the synthesized $CoFe_2O_4$, the catalytic oxidation of the typical peroxidase substrate TMB in the presence or absence of H_2O_2 was carried out (Figure 6A). Color changes of different systems can be observed from Figure 6B. The H_2O_2 + CF400 system and the H_2O_2 + TMB system show no absorption, while the TMB + H_2O_2 + CF400 system shows an obvious absorption peak at 652 nm, which indicates CF400 could act as a peroxidase to oxidize TMB to produce a blue color in the presence of H_2O_2. Interesting, the TMB + CF400 system shows a weak absorption, indicating that CF400 could catalyze the oxidation of TMB in the absence of H_2O_2 to produce a blue dye. The oxidase-like activity for TMB oxidation may originate from their catalytic ability to reduce dissolved oxygen [4]. Additionally, the peroxidase mimetic catalytic activities of $CoFe_2O_4$ at the different synthesized temperatures were tested and compared through the catalytic oxidation of TMB in the presence of H_2O_2. It can be seen from Figure 6C that CF300 exhibits the best peroxidase mimetic catalytic activity among the synthesized $CoFe_2O_4$ samples. The color changes of TMB with different $CoFe_2O_4$ samples are shown in Figure 6D. It can be found that all the $CoFe_2O_4$ samples prepared under different temperature possesses distinct peroxidase mimetic catalytic activities. CF300 system shows the most obvious blue color in comparison with that of CF400, CF500, CF600, and CF700. The most superior peroxidase mimetic activity of CF300 could be mainly owing to the rich catalytic activity sites provided by the largest specific surface area. As shown in Scheme 1, H_2O_2 reduction first takes place in the presence of chromogenic electron donor TMB, and then accelerates by partial electron transferring to the surface of CF300. Subsequently, the TMB is oxidized through one electron transfer and the color of the solution changes to blue.

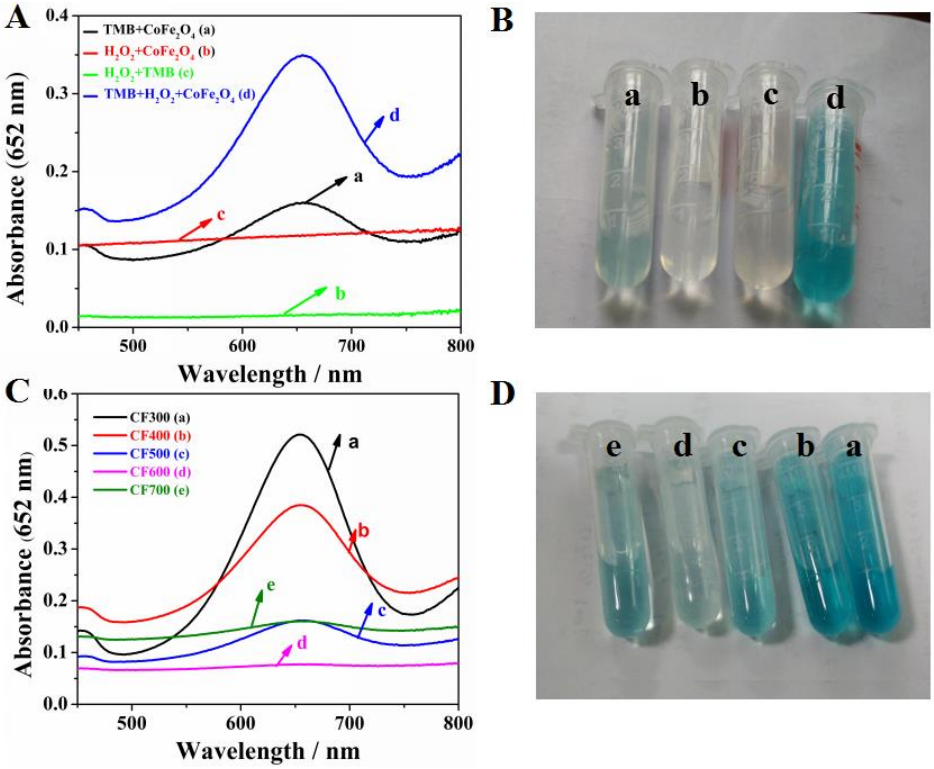

Figure 6. (**A**) UV-vis absorption spectra and (**B**) color changes in different reaction systems (a. TMB + CF400; b. H_2O_2 + CF400; c. H_2O_2 + TMB; d. TMB + H_2O_2 + CF400); (**C**) UV-vis absorption spectra and (**D**) color changes in the presence of different $CoFe_2O_4$ samples (a. CF300; b. CF400; c. CF500; d. CF600; e. CF700).

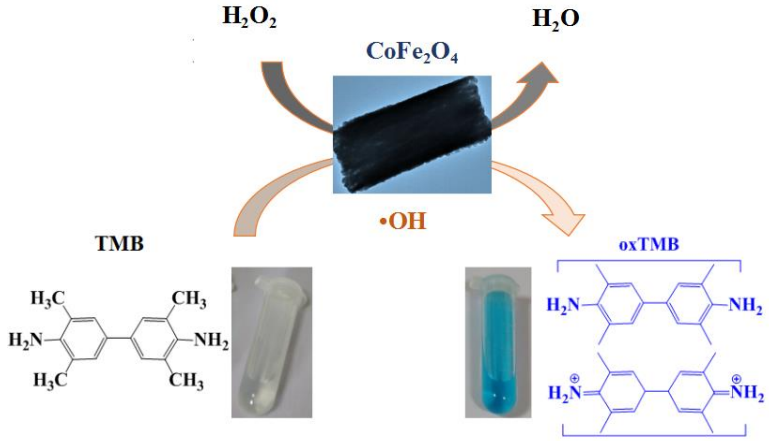

Scheme 1. Schematic illustration of peroxidase-like activity for CF300.

3.3. Optimal Condition for H_2O_2 Detection

In order to investigate the intrinsic catalytic activities of CF300, further experiments were carried out with various CF300 and H_2O_2 concentrations. Figure 7A shows that the peroxidase-like catalytic reaction rate increases with the elevating concentrations of CF300. For the convenience of operation, the concentration of CF300, 20 μg/mL, is used in the following experiments. Previous studies showed that the catalytic activities of horseradish peroxidase (HRP) could be inhibited at excess concentrations of H_2O_2 [53]. Figure 7B depicts the time course-dependent absorbance change at 652 nm for different concentrations of H_2O_2. The catalytic reaction rates increase with the increase of H_2O_2 concentration,

and no inhibition is found in the catalytic reaction at high H_2O_2 concentrations, which suggests a more stable catalytic activity for CF300 than that of HRP at high H_2O_2 concentration. The 4.0 mM is chosen as the optimal H_2O_2 concentration in the following experiments.

Similar to HRP and other mimetic enzymes, the catalytic relative activity of CF300 is dependent on the pH and temperature. Hence, we investigated the peroxidase-like activity of CF300 through varying the pH from 2 to 8 and the temperature from 20 °C to 40 °C. As shown in Figure 7C, the peroxidase-like activity of CF300 is much higher in weakly acidic solutions than in alkaline and neutral solutions. The maximum absorption for CF300 catalytic system appears at pH 3.0. In addition, the catalytic activity of CF300 is significantly affected by the temperature (Figure 7D). The catalytic activity offers an upgrade, firstly, with the increasing temperature. Subsequently, it starts to decline when the temperature is higher than 25 °C. Thus, for the convenience of operation, the 25 °C is selected as the experimental temperature.

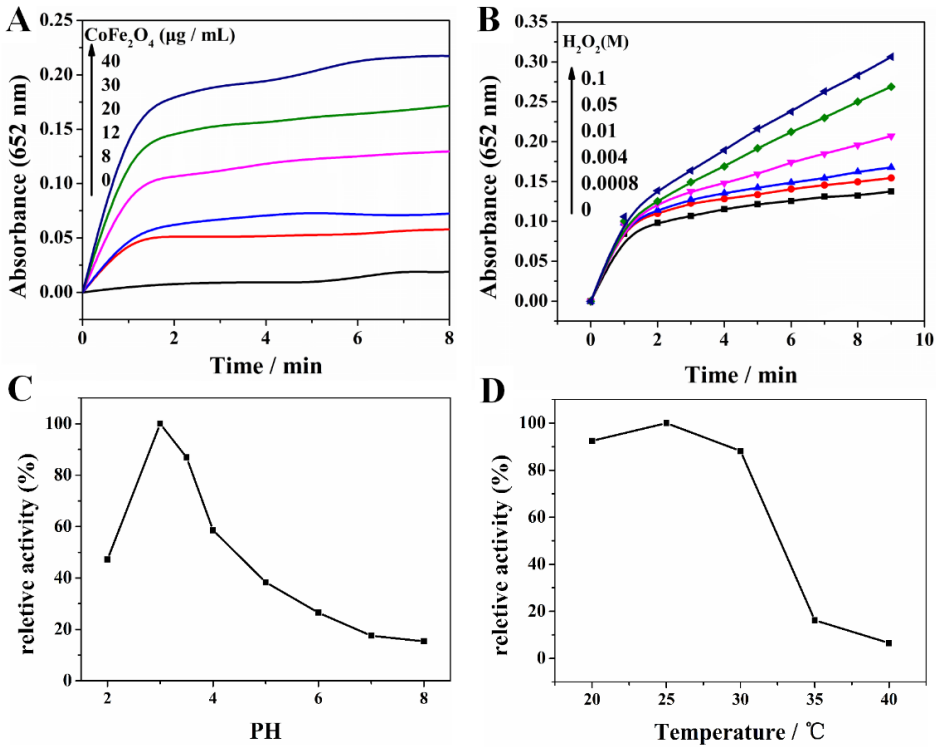

Figure 7. (**A**) Time-dependence absorbance at 652 nm of the 0.08 mM TMB reaction solution in the absence or presence of different doses of CF300 in 20 mM PBS (pH = 3.0) with 0.8 mM H_2O_2 at room temperature. (**B**) Time-dependence absorbance at 652 nm of the 0.4 mM TMB reaction solution in the absence or presence of different concentrations of H_2O_2 in 20 mM PBS (pH = 3.0) with 20 μg/mL CF300 at room temperature. Dependence of peroxidase-like activity of CF300 on pH (**C**) and temperature (**D**).

3.4. Catalytic Mechanism Study

In the presence of H_2O_2, CF300 could catalyze H_2O_2 to form the oxidized intermediate •OH radicals and subsequently oxidize TMB to produce blue dye. In order to confirm the catalytic mechanism, the •OH radical scavenger IPA was used in the CF300-TMB-H_2O_2 system, where IPA would easily react with •OH, leading to the decrease of the absorption at 652 nm and color fading of the system [2]. The corresponding chemical equation was:

$$CH_3CH(OH)CH_3 + \bullet OH \rightarrow CH_3CH(O)CH_3 + H_2O$$

Figure 8 shows an apparent color fading and absorption decrease at 652 nm for the system with IPA, confirming that CF300 could catalytically activate H_2O_2 to generate •OH radicals, and then oxidize TMB to produce a TMB oxide with blue color. Obviously, these results indicate that •OH radicals play a key role in the catalytic reaction.

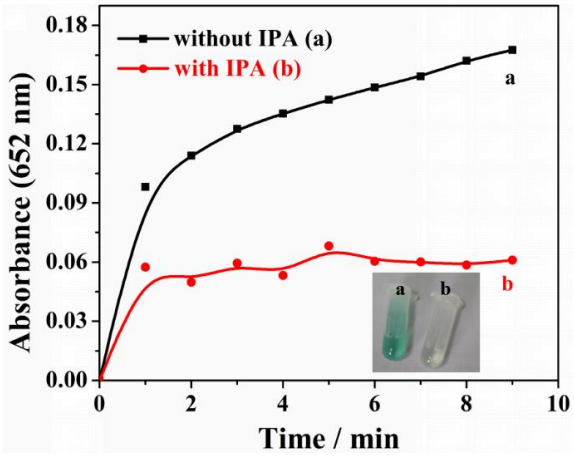

Figure 8. Time-dependent absorbance at 652 nm of the 0.4 mM TMB reaction solutions in the absence or presence of scavengers (IPA) in 20 mM PBS (pH = 3) with 20 μg/mL CF300 and 0.8 mM H_2O_2.

3.5. Steady-State Kinetic Assay

The catalytic steady-state kinetic of CF300 was evaluated by using TMB and H_2O_2 as substrates (Figure 9). The kinetic experiments were performed by only varying the concentration of TMB or H_2O_2 while keeping the other substrate concentration constant. As illustrated in Figure 9A,B, the Michaelis–Menten curves were obtained for both TMB and H_2O_2 in a certain concentration range. Accordingly, a series of initial reaction rates were obtained, and the double reciprocal plots (the reciprocal initial velocity vs. the reciprocal substrate concentration) were drawn as demonstrated in Figure 9C,D. The Michaelis–Menten constant (K_m) and maximal reaction velocity (V_{max}) for this system were calculated using Lineweaver–Burk plots and the Michaelis-Menten equation. The K_m (TMB) of the CF300 is 0.387 mM, which is lower than the reported value of HRP (0.434 mM), suggesting that CF300 has higher affinity for TMB than HRP (Table 2). On the other hand, the K_m (H_2O_2) of the CF300 is 8.89 mM, significantly higher than that of 3.7 mM for HRP [25], indicating that CF300 has lower affinity for H_2O_2. Additionally, the peroxidase-like catalytic reaction based on CF300 followed the typical Michaelis-Menten behavior [2,13] towards both substrates: TMB and H_2O_2. Additionally, the double-reciprocal plots (Figure 9C,D) exhibited the characteristic parallel lines of a ping-pong mechanism, indicating that CF300 bound and reacted with the first substrate and then released the first product before reacting with the second substrate, which is similar to that of HRP [2,25].

Table 2. Comparison of K_m and V_{max} between CF300 and HRP for H_2O_2 and TMB.

Catalysts	Substances	K_m (mM)	V_{max} (M/s)	References
$CoFe_2O_4$	H_2O_2	8.89	1.93×10^{-8}	This work
$CoFe_2O_4$	TMB	0.387	2.90×10^{-8}	This work
HRP	H_2O_2	3.7	8.71×10^{-8}	[10]
HRP	TMB	0.434	10.00×10^{-8}	[10]

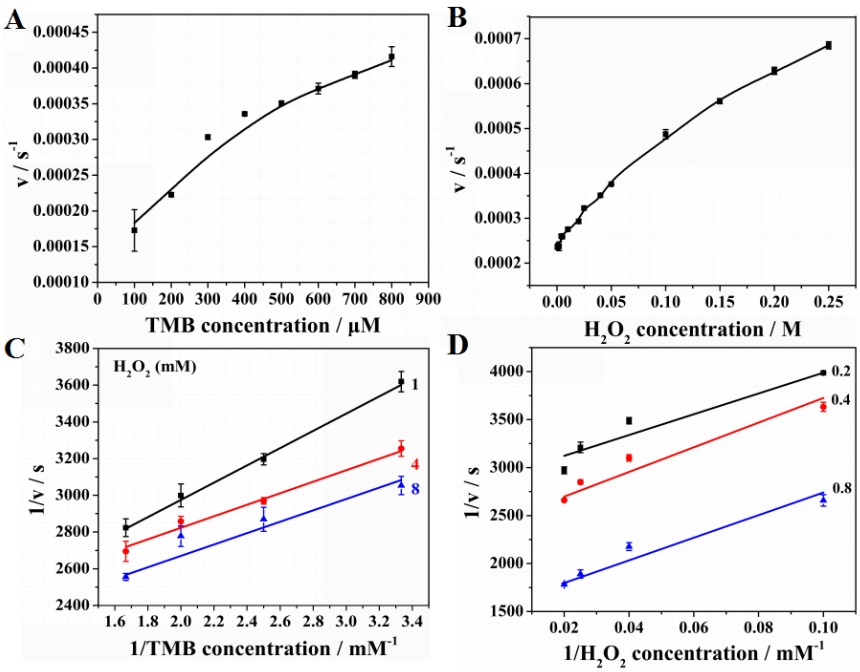

Figure 9. Steady-state kinetic assays of CF300, the reaction velocity (v) was measured using 20 μg/mL of CF300 in 20 mM PBS (pH = 3) at room temperature. The TMB concentration was varied and the concentration of H_2O_2 was 4 mM (**A**); the H_2O_2 concentration was varied and the concentration of TMB was 0.4 mM (**B**); and the double-reciprocal plots of peroxidase-like activity of CF300 with a fixed concentration of one substrate relative to varying concentration of the other substrate (**C**,**D**).

3.6. Detection of H_2O_2 and Oxidative Degradation of Methylene Blue

On the basis that peroxidase mimics the activity of the $CoFe_2O_4$ materials, we developed a facile and label-free colorimetric approach to detect H_2O_2. As shown in Figure 10, a typical H_2O_2 concentration response curve under the optical conditions is measured. The detection range for H_2O_2 is from 0.02 to 6 mM. The linear regression equation is A_{652nm} = 0.18388 + 0.0049C (mM), with a correlation coefficient of 0.9945. The detection limit for H_2O_2 is 0.02 mM, suggesting that the optical biosensing system built in this study can be applicable to the H_2O_2 determination.

Some studies confirmed that nanozymes could be used to remove pollutants from waste water [54–57]. Based on the excellent catalytic activity of CF300, we further investigated its MB degradation ability. Similar to other enzyme mimic reactions, the maximum UV-vis absorption (A_{max}) of MB aqueous solution is located at 665 nm [44]. Figure 11A shows the UV-vis absorption spectra of MB aqueous solution in the presence of CF300 and H_2O_2 at different reaction time. A sharp decrease for the absorption intensity of MB is observed with the increasing reaction time, the band at 665 nm become very weak and broad, and the removal rate of MB can reach 91.2% at 10 h (Figure 11B), suggesting that the MB has nearly completed degradation.

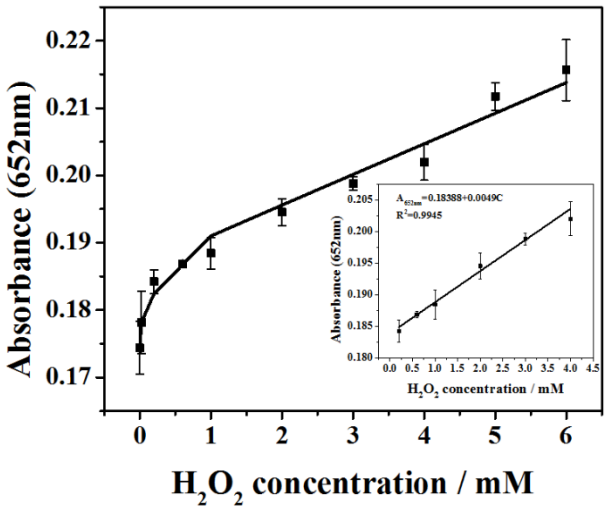

Figure 10. A concentration response curve H_2O_2 detection. Inset: the linear calibration plot.

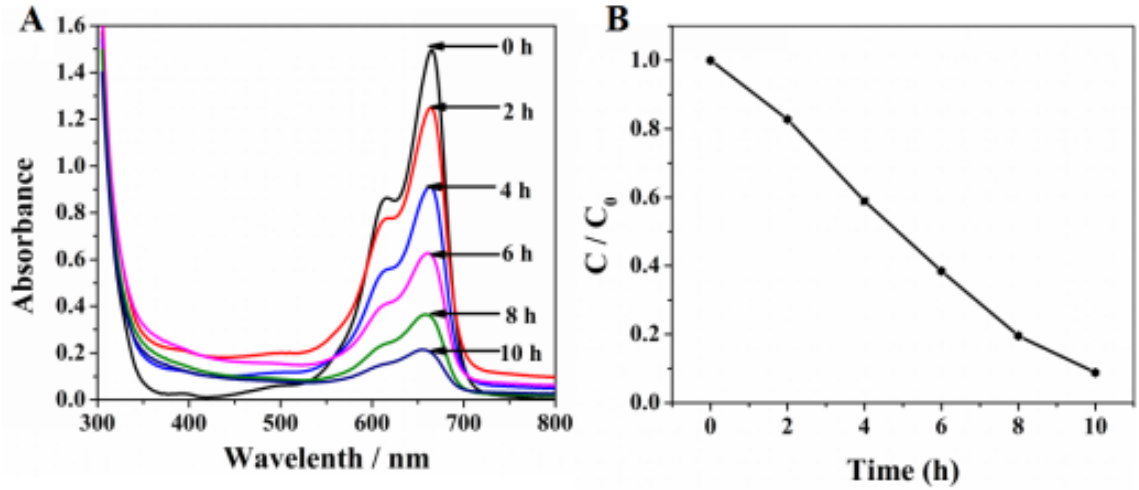

Figure 11. (**A**) UV-vis spectra obtained during the MB oxidative degradation over CF300; and (**B**) the MB degradation rate at various reaction time.

4. Conclusions

In summary, we developed a simple and controllable method for porous $CoFe_2O_4$ preparation. The specific surface area of $CoFe_2O_4$ materials was dependent on the annealing temperature and the CF300 exhibited a much higher specific surface area (204.1 m^2 g^{-1}) than other $CoFe_2O_4$ samples. The large specific surface area of CF300 endowed them more actives which resulted in the enhanced intrinsic peroxidase mimics activity. Additionally, based on the peculiarity, CF300 had excellent catalytic activity for the degradation of MB. Owing to the facile preparation, low cost, large specific surface area, and magnetic properties, the present $CoFe_2O_4$ showed great potential for applications in environmental protection, biomedical analysis, and other related areas.

Supplementary Materials: The following are available online at http://www.mdpi.com/2079-4991/8/7/451/s1.

Author Contributions: G.W. (Guizhen Wang) conceived and designed the experiments; L.W., G.W. (Gengping Wan), and S.S. performed the experiments; L.W., K.W., Z.H., X.X., Y.T., N.H., and Y.S. analyzed the data; G.W. (Guizhen Wang) contributed reagents, materials, and analysis tools; and G.W. (Guizhen Wang) and L.W. wrote the paper.

Acknowledgments: This work was financially supported by the National Natural Science Foundation of China (11564011, 21706046, 51362010) and the Natural Science Foundation of Hainan Province (514207, 514212).

Conflicts of Interest: The authors declare no conflict of interest.

References

1. Wang, N.; Sun, J.; Chen, L.; Fan, H.; Ai, S. A $Cu_2(OH)_3Cl$-CeO_2 nanocomposite with peroxidase-like activity, and its application to the determination of hydrogen peroxide, glucose and cholesterol. *Microchim. Acta* **2015**, *182*, 1733–1738. [CrossRef]
2. Yu, Y.; Ju, P.; Zhang, D.; Han, X.; Yin, X.; Zheng, L.; Sun, C. Peroxidase-like activity of $FeVO_4$ nanobelts and its analytical application for optical detection of hydrogen peroxide. *Sens. Actuators B Chem.* **2016**, *233*, 162–172. [CrossRef]
3. Wei, H.; Wang, E. Nanomaterials with enzyme-like characteristics (nanozymes): Next-generation artificial enzymes. *Chem. Soc. Rev.* **2013**, *42*, 6060–6093. [CrossRef] [PubMed]
4. Qiao, F.; Chen, L.; Li, X.; Li, L.; Ai, S. Peroxidase-like activity of manganese selenide nanoparticles and its analytical application for visual detection of hydrogen peroxide and glucose. *Sens. Actuators B Chem.* **2014**, *193*, 255–262. [CrossRef]
5. Yang, Z.; Ji, H. 2-Hydroxypropyl-β-cyclodextrin polymer as a mimetic enzyme for mediated synthesis of benzaldehyde in water. ACS. *Sustain. Chem. Eng.* **2013**, *1*, 1172–1179. [CrossRef]
6. Song, Y.; Qu, K.; Zhao, C.; Ren, J.; Qu, X. Graphene oxide: Intrinsic peroxidase catalytic activity and its application to glucose detection. *Adv. Mater.* **2010**, *22*, 2206–2210. [CrossRef] [PubMed]
7. Chen, X.; Zhou, X.; Hu, J. Pt–DNA complexes as peroxidase mimetics and their applications in colorimetric detection of H_2O_2 and glucose. *Anal. Methods* **2012**, *4*, 2183–2187. [CrossRef]
8. Khorshid, A.; Amin, R.; Issa, Y.M. Fabrication of a novel highly selective and sensitive nano-molar Cu(I), Cu(II) membrane sensors based on thiosemicarbazide and acetaldehydethiosemicarbazone copper complexes. *J. Chem. Acta* **2012**, *1*, 52–58.
9. Zhang, T.; Lu, Y.; Luo, G. Synthesis of hierarchical iron hydrogen phosphate crystal as a robust peroxidase mimic for stable H_2O_2 detection. *ACS Appl. Mater. Interfaces* **2014**, *6*, 14433–14438. [CrossRef] [PubMed]
10. Luo, W.; Zhu, C.; Su, S.; Li, D.; He, Y.; Huang, Q.; Fan, C. Self-catalyzed, self-limiting growth of glucose oxidase-mimicking gold nanoparticles. *ACS Nano* **2010**, *4*, 7451–7458. [CrossRef] [PubMed]
11. Tian, R.; Sun, J.; Qi, Y.; Zhang, B.; Guo, S.; Zhao, M. Influence of VO_2 nanoparticle morphology on the colorimetric assay of H_2O_2 and glucose. *Nanomaterials* **2017**, *7*, 347. [CrossRef] [PubMed]
12. Li, N.; Wu, D.; Hu, N.; Fan, G.; Li, X.; Sun, J.; Chen, X.; Suo, Y.; Li, G.; Wu, Y. Effective enrichment and detection of trace polycyclic aromatic hydrocarbons in food samples based on magnetic covalent organic framework hybrid microspheres. *J. Agric. Food Chem.* **2018**, *66*, 3572–3580. [CrossRef] [PubMed]
13. Zhan, T.; Kang, J.; Li, X.; Pan, L.; Li, G.; Hou, W. NiFe layered double hydroxide nanosheets as an efficiently mimic enzyme for colorimetric determination of glucose and H_2O_2. *Sens. Actuators B Chem.* **2018**, *255*, 2635–2642. [CrossRef]
14. Kotov, N.A. Chemistry.inorganic nanoparticles as protein mimics. *Science* **2010**, *330*, 188–189. [CrossRef] [PubMed]
15. Jin, L.; Meng, Z.; Zhang, Y.; Cai, S.; Zhang, Z.; Li, C.; Shang, L.; Shen, Y. Ultrasmall Pt nanoclusters as robust peroxidase mimics for colorimetric detection of glucose in human serum. *ACS Appl. Mater. Interfaces* **2017**, *9*, 10027–10033. [CrossRef] [PubMed]
16. Xiang, Z.; Wang, Y.; Ju, P.; Zhang, D. Optical determination of hydrogen peroxide by exploiting the peroxidase-like activity of $AgVO_3$ nanobelts. *Microchim. Acta* **2015**, *183*, 457–463. [CrossRef]
17. Liu, X.; Wang, Q.; Zhao, H.; Zhang, L.; Su, Y.; Lv, Y. BSA-templated MnO_2 nanoparticles as both peroxidase and oxidase mimics. *Analyst* **2012**, *137*, 4552–4558. [CrossRef] [PubMed]
18. Han, L.; Shi, J.; Liu, A. Novel biotemplated MnO_2 1D nanozyme with controllable peroxidase-like activity and unique catalytic mechanism and its application for glucose sensing. *Sens. Actuators B Chem.* **2017**, *252*, 919–926. [CrossRef]
19. Han, L.; Zhang, H.; Chen, D.; Li, F. Protein-directed metal oxide nanoflakes with tandem enzyme-like characteristics: Colorimetric glucose sensing based on one-pot enzyme-free cascade catalysis. *Adv. Funct. Mater.* **2018**, *28*, 1800018. [CrossRef]

20. Peng, H.; Lin, D.; Liu, P.; Wu, Y.; Li, S.; Lei, Y.; Chen, W.; Chen, Y.; Lin, X.; Xia, X.; et al. Highly sensitive and rapid colorimetric sensing platform based on water-soluble WO_x quantum dots with intrinsic peroxidase-like activity. *Anal. Chim. Acta* **2017**, *992*, 128–134. [CrossRef] [PubMed]
21. Karim, M.N.; Anderson, S.R.; Singh, S.; Ramanathan, R.; Bansal, V. Nanostructured silver fabric as a free-standing nanozyme for colorimetric detection of glucose in urine. *Biosens. Bioelectron.* **2018**, *110*, 8–15. [CrossRef] [PubMed]
22. André, R.; Natálio, F.; Humanes, M.; Leppin, J.; Heinze, K.; Wever, R.; Schröder, H.C.; Müller, W.E.G.; Tremel, W. V_2O_5 nanowires with an intrinsic peroxidase-like activity. *Adv. Funct. Mater.* **2011**, *21*, 501–509. [CrossRef]
23. Wei, H.; Wang, E. Fe_3O_4 magnetic nanoparticles as peroxidase mimetics and their applications in H_2O_2 and glucose detection. *Anal. Chem.* **2008**, *80*, 2250–2254. [CrossRef] [PubMed]
24. Wang, Q.; Zhang, X.; Huang, L.; Zhang, Z.; Dong, S. One-pot synthesis of Fe_3O_4 nanoparticle loaded 3D porous graphene nanocomposites with enhanced nanozyme activity for glucose detection. *ACS Appl. Mater. Interfaces* **2017**, *9*, 7465–7471. [CrossRef] [PubMed]
25. Gao, L.; Zhuang, J.; Nie, L.; Zhang, J.; Zhang, Y.; Gu, N.; Wang, T.; Feng, J.; Yang, D.; Perrett, S.; et al. Intrinsic peroxidase-like activity of ferromagnetic nanoparticles. *Nat. Nanotechnol.* **2007**, *2*, 577–583. [CrossRef] [PubMed]
26. Chen, S.; Hai, X.; Chen, X.-W.; Wang, J.-H. In situ growth of sSilver nanoparticles on graphene quantum dots for ultrasensitive colorimetric detection of H_2O_2 and glucose. *Anal. Chem.* **2014**, *86*, 6689–6694. [CrossRef] [PubMed]
27. Liu, J.; Hu, X.; Hou, S.; Wen, T.; Liu, W.; Zhu, X.; Yin, J.-J.; Wu, X. Au@Pt core/shell nanorods with peroxidase- and ascorbate oxidase-like activities for improved detection of glucose. *Sens. Actuators B Chem.* **2012**, *166–167*, 708–714. [CrossRef]
28. Peng, X.; Wan, G.; Wu, L.; Zeng, M.; Lin, S.; Wang, G. Peroxidase-like activity of Au@TiO_2 yolk-shell nanostructure and its application for colorimetric detection of H_2O_2 and glucose. *Sens. Actuators B Chem.* **2018**, *257*, 166–177. [CrossRef]
29. Qiao, F.; Wang, Z.; Xu, K.; Ai, S. Double enzymatic cascade reactions within FeSe-Pt@SiO_2 nanospheres: Synthesis and application toward colorimetric biosensing of H_2O_2 and glucose. *Analyst* **2015**, *140*, 6684–6691. [CrossRef] [PubMed]
30. Song, Y.; Wang, X.; Zhao, C.; Qu, K.; Ren, J.; Qu, X. Label-free colorimetric detection of single nucleotide polymorphism by using single-walled carbon nanotube intrinsic peroxidase-like activity. *Chem. Eur. J.* **2010**, *16*, 3617–3621. [CrossRef] [PubMed]
31. Lu, N.; Zhang, M.; Ding, L.; Zheng, J.; Zeng, C.; Wen, Y.; Liu, G.; Aldalbahi, A.; Shi, J.; Song, S. Yolk-shell nanostructured Fe_3O_4@C magnetic nanoparticles with enhanced peroxidase-like activity for label-free colorimetric detection of H_2O_2 and glucose. *Nanoscale* **2017**, *9*, 4508–4515. [CrossRef] [PubMed]
32. Zhang, L.; Hai, X.; Xia, C.; Chen, X.-W.; Wang, J.-H. Growth of CuO nanoneedles on graphene quantum dots as peroxidase mimics for sensitive colorimetric detection of hydrogen peroxide and glucose. *Sens. Actuators B Chem.* **2017**, *248*, 374–384. [CrossRef]
33. Chen, S.; Chi, M.; Zhu, Y.; Gao, M.; Wang, C.; Lu, X. A facile synthesis of superparamagnetic Fe_3O_4 nanofibers with superior peroxidase-like catalytic activity for sensitive colorimetric detection of l-cysteine. *Appl. Surf. Sci.* **2018**, *440*, 237–244. [CrossRef]
34. Feng, X.; Mao, G.Y.; Bu, F.X.; Cheng, X.L.; Jiang, D.M.; Jiang, J.S. Controlled synthesis of monodisperse $CoFe_2O_4$ nanoparticles by the phase transfer method and their catalytic activity on methylene blue discoloration with H_2O_2. *J. Magn. Magn. Mater.* **2013**, *343*, 126–132. [CrossRef]
35. Wang, G.; Gao, Z.; Tang, S.; Chen, C.; Duan, F.; Zhao, S.; Lin, S.; Feng, Y.; Zhou, L.; Qin, Y. Microwave absorption properties of carbon nanocoils coated with highly controlled magnetic materials by atomic layer deposition. *ACS Nano* **2012**, *6*, 11009–11017. [CrossRef] [PubMed]
36. Dobzhansky, T.; Holz, A.M.; Spassky, B. Magnetic-core/porous-shell $CoFe_2O_4/SiO_2$ composite nanoparticles as immobilized affinity supports for clinical immunoassays. *Adv. Funct. Mater.* **2007**, *17*, 976–982.

37. Zhang, X.; He, S.; Chen, Z.; Huang, Y. $CoFe_2O_4$ nanoparticles as oxidase mimic-mediated chemiluminescence of aqueous luminol for sulfite in white wines. *J. Agric. Food. Chem.* **2013**, *61*, 840–847. [CrossRef] [PubMed]
38. Shi, W.; Zhang, X.; He, S.; Huang, Y. $CoFe_2O_4$ magnetic nanoparticles as a peroxidase mimic mediated chemiluminescence for hydrogen peroxide and glucose. *Chem. Commun.* **2011**, *47*, 10785–10787. [CrossRef] [PubMed]
39. Fan, Y.; Huang, Y. The effective peroxidase-like activity of chitosan-functionalized $CoFe_2O_4$ magnetic nanoparticles as a peroxidase mimic mediated chemiluminescence for hydrogen peroxide and glucose nanoparticles for chemiluminescence sensing of hydrogen peroxide and glucose. *Analyst* **2012**, *137*, 1225–1231. [CrossRef] [PubMed]
40. Wan, G.; Yu, L.; Peng, X.; Wang, G.; Huang, X.; Zhao, H.; Qin, Y. Preparation and microwave absorption properties of uniform TiO_2@C core–shell nanocrystals. *RSC Adv.* **2015**, *5*, 77443–77448. [CrossRef]
41. Wang, L.; Zeng, Y.; Shen, A.; Zhou, X.; Hu, J. Three dimensional nano-assemblies of noble metal nanoparticle-infinite coordination polymers as specific oxidase mimetics for degradation of methylene blue without adding any cosubstrate. *Chem. Commun.* **2015**, *51*, 2052–2055. [CrossRef] [PubMed]
42. Liu, M.; Zhao, H.; Chen, S.; Yu, H.; Quan, X. Interface engineering catalytic graphene for smart colorimetric biosensing. *ACS Nano* **2012**, *6*, 3142–3151. [CrossRef] [PubMed]
43. Ai, L.; Li, L.; Zhang, C.; Fu, J.; Jiang, J. MIL-53(Fe): A metal–organic framework with intrinsic peroxidase-like catalytic activity for colorimetric biosensing. *Chem. Eur. J.* **2013**, *19*, 15105–15108. [CrossRef] [PubMed]
44. Prathap, M.U.A.; Kaur, B.; Srivastava, R. Hydrothermal synthesis of CuO micro-/nanostructures and their applications in the oxidative degradation of methylene blue and non-enzymatic sensing of glucose/H_2O_2. *J. Colloid Interface Sci.* **2012**, *370*, 11316–11319. [CrossRef] [PubMed]
45. Qu, Y.; Yang, H.; Yang, N.; Fan, Y.; Zhu, H.; Zou, G. The effect of reaction temperature on the particle size, structure and magnetic properties of coprecipitated $CoFe_2O_4$ nanoparticles. *Mater. Lett.* **2006**, *60*, 3548–3552. [CrossRef]
46. Shemer, G.; Tirosh, E.; Livneh, T.; Markovich, G. Tuning a colloidal synthesis to control Co^{2+} doping in ferrite nanocrystals. *J. Phys. Chem. C* **2015**, *111*, 14334–14338. [CrossRef]
47. Gandha, K.; Elkins, K.; Poudyal, N.; Liu, J.P. Synthesis and characterization of $CoFe_2O_4$ nanoparticles with high coercivity. *J. Appl. Phys.* **2015**, *117*, 17A736. [CrossRef]
48. Gao, Z.; Cui, F.; Zeng, S.; Guo, L.; Shi, J. A high surface area superparamagnetic mesoporous spinel ferrite synthesized by a template-free approach and its adsorptive property. *Microporous Mesoporous Mater.* **2010**, *132*, 188–195. [CrossRef]
49. Wang, G.; Gao, Z.; Wan, G.; Lin, S.; Yang, P.; Qin, Y. High densities of magnetic nanoparticles supported on graphene fabricated by atomic layer deposition and their use as efficient synergistic microwave absorbers. *Nano Res.* **2014**, *7*, 704–716. [CrossRef]
50. Wang, K.; Wan, G.; Wang, G.; He, Z.; Shi, S.; Wu, L.; Wang, G. The construction of carbon-coated Fe_3O_4 yolk-shell nanocomposites based on volume shrinkage from the release of oxygen anions for wide-band electromagnetic wave absorption. *J. Colloid Interface Sci.* **2018**, *511*, 307–317. [CrossRef] [PubMed]
51. Wang, Z.; Liu, X.; Lv, M.; Chai, P.; Liu, Y.; Zhou, X.; Meng, J. Preparation of one-dimensional $CoFe_2O_4$ nanostructures and their magnetic properties. *J. Phys. Chem. C* **2009**, *112*, 15171–15175. [CrossRef]
52. Qu, Y.; Zhang, D.; Wang, X.; Qiu, H.; Zhang, T.; Zhang, M.; Tian, G.; Yue, H.; Feng, S.; Chen, G. Porous $ZnFe_2O$ nanospheres as anode materials for Li-ion battery with high performance. *J. Alloy. Compd.* **2017**, *721*, 697–704. [CrossRef]
53. Nicell, J.A.; Wright, H. A model of peroxidase activity with inhibition by hydrogen peroxide. *Enzyme Microb. Technol.* **1997**, *21*, 302–310. [CrossRef]
54. Cai, Q.; Lu, S.; Liao, F.; Li, Y.; Ma, S.; Shao, M. Catalytic degradation of dye molecules and in situ SERS monitoring by peroxidase-like Au/CuS composite. *Nanoscale* **2014**, *6*, 8117–8123. [CrossRef] [PubMed]
55. Wu, X.; Zhang, Y.; Han, T.; Wu, H.; Guo, S.; Zhang, J. Composite of graphene quantum dots and Fe_3O_4 nanoparticles: Peroxidase activity and application in phenolic compound removal. *RSC Adv.* **2013**, *4*, 3299–3305. [CrossRef]

56. Pan, Y.; Li, N.; Mu, J.; Zhou, R.; Xu, Y.; Cui, D.; Wang, Y.; Zhao, M. Biogenic magnetic nanoparticles from *Burkholderia* sp. YN01 exhibiting intrinsic peroxidase-like activity and their applications. *Appl. Microbiol. Biotechnol.* **2015**, *99*, 703–715. [CrossRef] [PubMed]
57. Janoš, P.; Kuráň, P.; Pilařová, V.; Trögl, J.; Šťastný, M.; Pelant, O.; Henych, J.; Bakardjieva, S.; Životský, O.; Kormunda, M. Magnetically separable reactive sorbent based on the CeO_2/γ-Fe_2O_3 composite and its utilization for rapid degradation of the organophosphate pesticide parathion methyl and certain nerve agents. *Chem. Eng. J.* **2015**, *262*, 747–755. [CrossRef]